Biophysical *Journal*
Article

Biophysical Society

Mechanosensitive axon outgrowth mediated by L1-laminin clutch interface

Kouki Abe,[1] Kentarou Baba,[1] Liguo Huang,[1] Koay Teng Wei,[1] Kazunori Okano,[2] Yoichiroh Hosokawa,[2] and Naoyuki Inagaki[1,*]

[1]Laboratory of Systems Neurobiology and Medicine, Division of Biological Science and [2]Bio-processing Engineering Laboratory, Division of Materials Science, Nara Institute of Science and Technology, Ikoma, Japan

ABSTRACT Mechanical properties of the extracellular environment modulate axon outgrowth. Growth cones at the tip of extending axons generate traction force for axon outgrowth by transmitting the force of actin filament retrograde flow, produced by actomyosin contraction and F-actin polymerization, to adhesive substrates through clutch and cell adhesion molecules. A molecular clutch between the actin filament flow and substrate is proposed to contribute to cellular mechanosensing. However, the molecular identity of the clutch interface responsible for mechanosensitive growth cone advance is unknown. We previously reported that mechanical coupling between actin filament retrograde flow and adhesive substrates through the clutch molecule shootin1a and the cell adhesion molecule L1 generates traction force for axon outgrowth and guidance. Here, we show that cultured mouse hippocampal neurons extend longer axons on stiffer substrates under elastic conditions that correspond to the soft brain environments. We demonstrate that this stiffness-dependent axon outgrowth requires actin-adhesion coupling mediated by shootin1a, L1, and laminin on the substrate. Speckle imaging analyses showed that L1 at the growth cone membrane switches between two adhesive states: L1 that is immobilized and that undergoes retrograde movement on the substrate. The duration of the immobilized phase was longer on stiffer substrates; this was accompanied by increases in actin-adhesion coupling and in the traction force exerted on the substrate. These data suggest that the interaction between L1 and laminin is enhanced on stiffer substrates, thereby promoting force generation for axon outgrowth.

SIGNIFICANCE Axonal growth cones respond to mechanical properties in their environment. A molecular clutch between F-actin retrograde flow and the adhesive substrate is proposed to contribute to cellular mechanosensing. However, the molecular identity of the clutch interface responsible for mechanosensitive growth cone advance is unknown. We show that substrate-stiffness-dependent axon outgrowth of cultured hippocampal neurons requires actin-adhesion coupling mediated by the clutch molecule shootin1a, the cell adhesion molecule L1, and the adhesive ligand laminin. The interaction between L1 and laminin was enhanced on stiffer substrates, thereby increasing the efficiency of force generation by growth cones. Thus, these data demonstrate that the stiffness-dependent L1-laminin interaction mediates this mechanosensitivity of the growth cone machinery for axon outgrowth of hippocampal neurons.

INTRODUCTION

Growth cones located at the tip of extending axons probe extracellularly presented local cues and guide long-distance axonal extension toward their target cells and tissues (1–5). Concerning the force to drive growth cone migration, actin filaments (F-actins) polymerize at their leading edge and disassemble proximally, which, together with myosin II activity, drives retrogradely directed F-actin retrograde flow (6–9). Mechanical coupling between the F-actin retrograde flow and adhesive substrates by clutch and cell adhesion molecules is thought to generate force for axon outgrowth (10–12). The actin-adhesion coupling transmits the force of F-actin retrograde flow produced by actomyosin contraction and F-actin polymerization to the substrate as traction force; concurrently, it reduces the speed of the F-actin flow (10–12), thereby converting actin polymerization into the force that protrudes the leading-edge membrane (13).

Accumulating evidence suggests that growth cones respond not only to chemical ligands but also to mechanical properties of their environment (5,14,15). Brain tissue is relatively soft (0.1–10 kPa) compared to other tissues,

Submitted March 9, 2021, and accepted for publication August 4, 2021.

*Correspondence: ninagaki@bs.naist.jp

Editor: Guy Genin.

https://doi.org/10.1016/j.bpj.2021.08.009

such as muscle (10–100 kPa) and connective tissues (100–1000 kPa) (16–18), and heterogeneous depending on developmental stages and regions (19–22). Neurons cultured on adhesive substrates with differing stiffness extend axons of different lengths depending on the cell type (23–26). Consistent with this, growth cones produce different amplitudes of traction force depending on the stiffness of the substrate (14,24). As a possible mechanism for such mechanosensitivity, the molecular clutch between F-actin retrograde flow and the adhesive substrate is thought to contribute to cellular mechanosensing (14,27,28). Previous studies reported that mechanosensitive ion channels contribute to the regulation of mechanosensitive growth cone advance (15,25). On the other hand, the molecular identity of the clutch interface responsible for mechanosensitive growth cone advance is unclear.

L1 is a single-pass transmembrane cell adhesion molecule of the immunoglobulin superfamily that is expressed predominantly in the nervous system and is involved in axon outgrowth and guidance (29,30). L1 binds directly to the extracellular matrix protein laminin (31,32) and mediates axon outgrowth on laminin (33). Recently, we reported that L1 and the clutch molecule shootin1a play key roles in growth cone migration regulated by diffusible and substrate-bound chemical ligands (31,34). Shootin1a interacts with F-actin retrograde flow through its direct association with the actin-interacting protein cortactin (35); it also interacts directly with L1 (34), thereby mechanically coupling the F-actin flow with the adhesive substrates (34,36). The attractive axon guidance molecule netrin-1 induces Pak1-mediated shootin1a phosphorylation (12); this, in turn, enhances shootin1a-mediated clutch coupling within growth cones and produces directional force for netrin-1-induced axon guidance (34). In addition, L1 at the growth cone membrane undergoes grip and retrograde slip on laminin; the directional force for laminin-induced axon guidance is exerted on the substrates by the grip and slip of L1, which occur asymmetrically under the growth cone (31).

Here, we show that cultured hippocampal neurons extend longer axons on stiffer substrates and that the stiffness-dependent growth cone advance requires actin-adhesion coupling mediated by shootin1a, L1, and laminin on the substrate. The duration of the grip phase of L1 was longer on stiffer substrates; this was accompanied by increases in actin-adhesion coupling and the traction force exerted on the substrate. These data indicate that the stiffness-dependent L1-laminin interaction mediates this mechanosensitivity of the growth cone machinery for axon outgrowth of hippocampal neurons.

MATERIALS AND METHODS

Cell culture and transfection

All relevant aspects of the experimental procedures were approved by the Institutional Animal Care and Use Committee of Nara Institute of Science and Technology. Hippocampal neurons prepared from E16 mouse embryos were seeded on polyacrylamide gels coated either sequentially with 100 μg/mL poly-D-lysine (PDL) (catalog number: P-6407; Sigma, St. Louis, MO) and 50 μg/mL laminin (catalog number: 120-05751; Wako Pure Chemical Industries, Osaka, Japan) or with PDL alone and cultured in neurobasal medium (catalog number: 21103049; Thermo Fisher Scientific, Waltham, MA) containing B-27 supplement (catalog number: 17504044; Thermo Fisher Scientific) and 1 mM glutamine (catalog number: 13012-92; nacalai tesque, Kyoto, Japan) without a glia feeder layer, as described (31). Neurons were transfected with plasmid DNA using Nucleofector (Lonza, Basel, Switzerland) before plating. A polypeptide including residues 1–125 of shootin1a (shootin1a (1–125)), which acts as shootin1a dominant-negative mutant (shootin1a-DN), was generated previously (34). pCAGGS-myc was used to overexpress myc-shootin1a (1–125) or myc-GST under the β-actin promoter as described (37). For analyses of axon outgrowth on elastic substrates, we used hippocampal neurons prepared from wild-type (WT) or shootin1 knockout (KO) E16.5 mouse embryos. The generation of shootin1 KO mice is described elsewhere (34). Male and female shootin1 heterozygous mice were mated to obtain WT and shootin1 KO mouse embryos; the offspring genotypes were checked by PCR with the following primers: genotyping F1 (5′-CAGACTGCTACCCACTACCCCCTAC-3′), genotyping R1 (5′-CCTAGAGCTGGACAGCGGATCTGAG-3′), genotyping F2 (5′-CCCAGAAAGCGAAGGAACAAAGCTG-3′), and genotyping R2 (5′-ACCTTGCTCCTTCAAGCTGGTGATG-3′).

Substrate preparation

A glass bottom dish (35 mm, catalog number: 81218-200; Ibidi, Gräfelfing, Germany) was treated with 0.1 N NaOH for 15 min; then, 3-aminopropyltrimethyoxysilane (catalog number: A3648; Sigma-Aldrich) was added to 0.1 N NaOH on the glass bottom dish at a final concentration of 2% (v/v) and incubated for 15 min. After washing with H_2O three times, 0.5% glutaraldehyde (catalog number: G5882; Sigma-Aldrich) solution in phosphate-buffered saline (PBS) was dropped onto the glass bottom dish and incubated for 30 min. The dish was then washed with H_2O three times and dried before use. Acrylamide monomer (catalog number: 00809-85; nacalai tesque) and bis-acrylamide monomer (catalog number: 22402-02; nacalai tesque) solutions were mixed to give the compositions listed in Table S1. After the addition of H_2O, the mixture was degassed for 15 min and incubated at 28°C for 30 min. After the addition of 2 μL of 10% APS (ammonium persulfate) (catalog number: 17131101; GE Healthcare, Chicago, IL) and 2 μL of TEMED (N,N,N′,N′-tetramethylethylenediamine) (catalog number: 33401-72; nacalai tesque) to the solution, 7 μL of the mixture was placed on an 18-mm glass coverslip (catalog number: C018001; Matsunami, Osaka, Japan). The glass bottom dish was then affixed inversely to the coverslip and incubated for 2 h at 28°C to form a polyacrylamide gel. After removal of the coverslip, the gel was washed with H_2O three times and incubated in PBS at 4°C overnight. The gel was then cross-linked with 1 mM Sulfo-SANPAH (sulfosuccinimidyl 6-(4′-azido-2′-nitrophenylamino)hexanoate) (catalog number: 22589; Pierce Biotechnology, Rockford, IL) by UV irradiation for 10 min and washed with PBS three times. PDL solution (100 μg/mL) was applied to the gel and incubated at 37°C overnight. After three washes with PBS, laminin solution, filtrated through a polyvinylidene fluoride membrane with 0.1 μm pore size (catalog number: IPVH00010; Millipore, Burlington, MA) to remove aggregated laminin and then diluted to 50 μg/mL, was applied to the PDL-coated gel at 37°C overnight. The gel was washed with PBS three times and used for cell culture.

The thickness of the gels prepared by this method was 35 $\pm$ 6.6 μm (mean $\pm$ SD), which is very thin compared to those used in other studies (38–40). Thin gels are required to obtain clear signals of HaloTag-actin and L1-HaloTag for reliable speckle imaging analyses in Figs. 3, 4, and 5 but are likely to be more affected by regional heterogeneities in the polymerization and thickness of polyacrylamide gels, which occur intrinsically during polymerization and produce regionally variable stiffness. We

therefore used the percentage of acrylamide, not Young's modulus, to describe gel stiffness.

Measurement of substrate stiffness

Measurement of substrate stiffness was conducted by atomic force microscopy (AFM) using a NanoWizard 4 (JPK Instruments, Berlin, Germany) with a tipless cantilever (catalog number: HQ:CSC38/Cr-Au; Mikro-Masch, Sofia, Bulgaria). A polystyrene sphere bead with a diameter of 39.33 ± 0.35 μm (Duke Standards, catalog number: 4240A; Thermo Fisher Scientific) was glued to the cantilever with a commercial epoxy resin adhesive. The spring constant after the bead bonding was estimated to be 0.05 N/m. The measurement was conducted on 3.5, 8, and 16% polyacrylamide gels put in PBS. Force curves were obtained by a force mapping mode with set point at 2 nN and approach velocity at 2 μm/s. Young's modulus of the polyacrylamide gels was determined by fitting force curves in the entire observation data to Hertz's equation for spherical indentation (20):

$$F = \frac{4}{3}\frac{E}{1-\nu^2}r^{1/2}\delta^{3/2}, \quad (1)$$

where F is the load force, δ is the indentation depth, E is Young's modulus, ν is Poisson's ratio, and r is the radius of the spherical probe. We set Poisson's ratio to 0.3 for all polyacrylamide gels (41).

Fluorescent speckle microscopy and grip and slip analysis

Fluorescent speckle imaging and speckle tracking analyses of HaloTag-actin and L1-HaloTag were performed as described previously (31). Neurons expressing HaloTag-actin or L1-HaloTag were treated with HaloTag tetramethylrhodamine ligand (catalog number: G2991; Promega, Madison, WI) at 1:1500 dilution in the culture medium and incubated for 1 h at 37°C. The ligand was then washed with PBS three times, and the cells were incubated with the culture medium for 30 min at 37°C. Before observation, the medium was replaced with L15 medium (catalog number: 21083027; Thermo Fisher Scientific) including B-27 supplement and 1 mM glutamine. The fluorescent features of L1-HaloTag in filopodia and lamellipodia were observed using a fluorescence microscope (Axio Observer.Z1; Carl Zeiss, Oberkochen, Germany) equipped with a complementary metal-oxide-semiconductor camera (ORCA Flash4.0 V2; Hamamatsu Photonics, Hamamatsu, Japan) and a Plan-Apochromat 100×/1.40 oil objective lens (Carl Zeiss). Fluorescent signals of L1-HaloTag were monitored at 5-s intervals.

We use the terms "grip" and "slip" to describe the movement of L1-HaloTag. "Grip vs. slip" was used by Jurado et al. to describe the degree of interaction between the cell adhesion and adhesive substrate in fish keratocytes (42). Subsequently, Aratyn-Schau and Gardel used "frictional slip" to describe the experimentally observed retrograde movement of focal adhesions (including integrin) of human osteosarcoma cells on adhesive substrates (43). Based on their concept and terms, we previously called L1 molecules that undergo retrograde movement on adhesive substrates as being in the "slip" phase and those immobilized on the substrates as being in the "grip" phase (31); we follow this terminology here. On the other hand, the clutch model developed by Chan and Odde (14) and advanced by Roca-Cusachs et al. (28) uses similar terms in a different context in clutch engagement; it uses "frictional slippage" and "load and fail" to describe low cell-matrix adhesion and high cell-matrix adhesion states, respectively (14,28). Note, therefore, that "grip" versus "slip" in this work describes the experimentally observed L1 movement, not the "frictional slippage" versus "load and fail" regimes.

For the grip and slip analysis, L1 puncta that were visible for at least 10 s (two intervals) were analyzed, and immobile signals were defined as L1 in grip phase, whereas those that flowed retrogradely were defined as L1 in slip phase.

Immunocytochemistry, immunoblot, and microscopy

Cultured neurons were fixed with 3.7% formaldehyde (catalog number: 16223-55; nacalai tesque) in PBS for 15 min on ice, treated for 15 min with 0.05% Triton X-100 in PBS on ice, and blocked by 10% fetal bovine serum in PBS for 1 h at room temperature. They were then stained with a mouse anti-βIII-tubulin antibody (monoclonal antibody, catalog number: 801201, lot no. B249869; BioLegend, San Diego, CA) at 1:1000 dilution, as described (31). Neurons overexpressing myc-GST or myc-shootin1a-DN were stained with anti-myc antibody (polyclonal antibody, catalog number: 562-5, lot No. 1901227; MBL, Tokyo, Japan). Immunoblot was performed using goat anti-NCAM-L1 (C-2) antibody (monoclonal antibody, catalog number: sc-514360; Santa Cruz Biotechnology, Santa Cruz, CA), mouse anti-cortactin antibody (clone 4F11, monoclonal antibody, catalog number: 05-180, lot no. 3073971; Millipore), rabbit anti-shootin1a peptide sequence antibody (34), and mouse anti-actin antibody (clone C4, monoclonal antibody, catalog number: MAB1501, lot No. 3538098; Millipore) as described (37). Fluorescence images of neurons were acquired using a fluorescence microscope (BZ-X700; Keyence, Osaka, Japan) equipped with a CFI PlanApo λ 20×/0.75 objective lens (Nikon, Tokyo, Japan).

Traction force microscopy

Traction force microscopy was performed as described (12,31). Briefly, neurons were cultured on laminin-coated 3.5, 8, and 16% polyacrylamide gels embedded with 200-nm fluorescent microspheres (200 nm diameter, catalog number: F8810; Thermo Fisher Scientific). Time-lapse imaging of fluorescent beads and growth cones was performed at 37°C using a confocal microscope (LSM710; Carl Zeiss) equipped with a C-Apochromat 63×/1.2 W Korr objective lens. The growth cone area was determined from differential interference contrast images. Traction force under growth cones was estimated from the displacement of two-dimensional-distributed beads: we applied the Ridge regularization algorithm for the force estimation (12,44). To compare the forces under different conditions, the magnitudes of the force vectors of the individual growth cones were statistically analyzed and expressed as means ± standard error (SE), separately. They were also analyzed by an unpaired Student's t-test.

Quantification of laminin on polyacrylamide gels

Alexa-555-conjugated laminin (50 μg/mL) was prepared as described (45) and incubated on PDL-coated polyacrylamide gels overnight at 37°C. The gels were then washed with PBS three times. Fluorescent signals of Alexa-555 laminin on 3.5, 8, and 16% gels were imaged by a fluorescence microscope (BZ-X710; Keyence) equipped with a CFI PlanApo λ 10×/0.45 objective lens (Nikon). The fluorescence intensity of Alexa-555-conjugated laminin was quantified by ImageJ 1.53c. The relative fluorescence intensity was calculated by dividing each value of fluorescence intensity by the maximal value of intensity in individual experiments ($n = 8$).

Statistical analyses

Significance was determined by an unpaired Student's t-test using Excel 2016 (Microsoft, Redmond, WA). For multiple comparisons, we used one-way ANOVA with Tukey's post hoc test using GraphPad Prism 7.

RESULTS

Hippocampal neurons extend longer axons on stiffer laminin-coated substrates

To examine mechanosensitive axon outgrowth, we cultured hippocampal neurons for 48 h on 3.5, 8, and 16% polyacrylamide gels and on glass, which were coated sequentially with PDL and laminin (Fig. 1 *A*). Stiffness of the 3.5, 8, and 16% gels examined by AFM was 72.8 ± 1.2, 1477 ± 35, and 3933 ± 120 Pa, respectively (Fig. S1 *A*), values that are approximately within the range of the stiffness of brain tissues (100–10,000 Pa) (16–18). The amount of coated laminin, quantified using Alexa555-conjugated laminin, was similar on 3.5, 8, and 16% gels (Fig. S1 *B*). Remarkably, neurons extended significantly longer axons on stiffer gels; axon lengths on 3.5, 8, and 16% gels were 124.6 ± 3.5, 153.1 ± 5.5, and 185.0 ± 6.6 μm, respectively (Fig. 1, *A* and *B*). Neurons extended axons of similar length on 16% gel and on glass, suggesting that the stiffness effect reaches a plateau on the 16% gel (Fig. 1, *A* and *B*). On the other hand, total neurite length showed a slight increase on 16% gel and glass; the total lengths were 240.5 ± 7.1, 235.1 ± 9.0, 279.6 ± 9.8, and 340.6 ± 11 μm on 3.5, 8, and 16% gels on and glass, respectively (Fig. S1 *C*). Notably, axon length was decreased, and neurons did not show the stiffness dependency of axon outgrowth when they were cultured on gels without laminin (coated only with PDL) (Fig. 1, *B* and *C*), indicating that stiffer substrates promote axon outgrowth in a laminin-dependent manner.

Mechanosensitive axon outgrowth requires shootin1a-mediated actin-adhesion coupling

As shootin1a promotes axon outgrowth through its clutch linkage between F-actin retrograde flow and laminin on the substrate (31), the laminin dependency of the mechanosensitive axon outgrowth raised the possibility that the actin-adhesion coupling involving shootin1a, cortactin, L1, and laminin (Fig. 2 *A*) mediates this mechanosensitivity. To examine this possibility, we cultured hippocampal neurons prepared from shootin1 KO mice (34). As shown in Fig. 2, *B* and *C*, shootin1 KO neurons on 3.5, 8, and 16% gels extended significantly shorter axons compared to control neurons. Furthermore, the stiffness-dependent axon outgrowth was abolished by shootin1 KO (Fig. 2 *C*), indicating that shootin1a is also involved in the mechanosensitive axon outgrowth.

To further analyze the role of shootin1a-mediated actin-adhesion coupling, we inhibited the interaction between shootin1a and L1 by overexpressing shootin1a-DN. We previously reported that a truncated polypeptide comprising residues 1–125 of shootin1a (shootin1a (1–125)) acts as a shootin1a-DN that inhibits the interaction between endogenous shootin1a and L1 (34). Overexpression of shootin1a-DN decreased axon length on 3.5, 8, and 16% gels and disrupted the stiffness-dependent axon outgrowth (Fig. 2, *D* and *E*). In addition, the expression levels of L1, cortactin, shootin1a, and actin in control neurons did not change on different elastic substrates (Fig. S1 *D*), thereby excluding the possibility that the stiffness-dependent axon outgrowth is mediated through a change in expression of these molecules. Together, these results indicate that mechanosensitive axon outgrowth requires shootin1a-mediated actin-adhesion coupling.

Increase in substrate stiffness promotes actin-adhesion coupling and traction force on the substrate

Because mechanosensitive axon outgrowth requires shootin1a-mediated actin-adhesion coupling, we next analyzed the influence of substrate stiffness on the efficiency of actin-adhesion coupling. To do this, the speed of F-actin retrograde flow was monitored in axonal growth cones by fluorescent speckle imaging of HaloTag-actin (Fig. 3 *A*; Video S1). An increase in actin-adhesion coupling can be

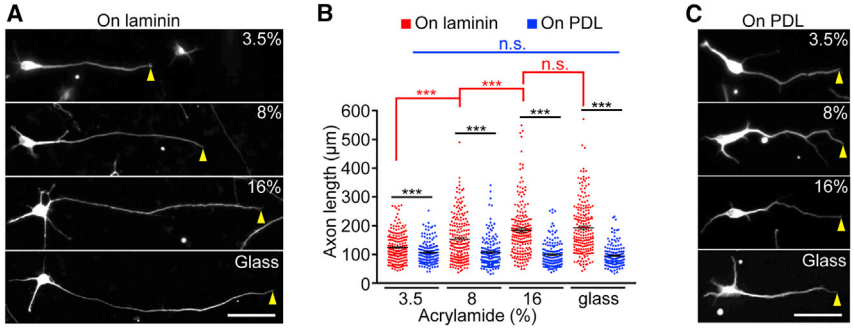

FIGURE 1 Hippocampal neurons extend longer axons on stiffer adhesive substrates. (*A*) Hippocampal neurons cultured on laminin-coated 3.5, 8, and 16% polyacrylamide gels and glasses for 48 h and stained with anti-βIII-tubulin antibody. Arrowheads indicate axonal tips. (*B*) Quantification of axon length of neurons on laminin-coated gels and glasses in (*A*) (3.5%, n = 202 neurons; 8%, n = 205 neurons; 16%, n = 199 neurons; glass, n = 203 neurons) and quantification of axon length of neurons on PDL-coated gels and glasses in (*C*) (3.5%, n = 152 neurons; 8%, n = 157 neurons; 16%, n = 151 neurons; glass, n = 153 neurons). (*C*) Hippocampal neurons cultured on PDL-coated 3.5, 8, and 16% polyacrylamide gels and glasses for 48 h and stained with anti-βIII-tubulin antibody. Arrowheads indicate axonal tips. Scale bars, 50 μm. Data in (*B*) represent means ± SE; ***$p < 0.01$; n.s., nonsignificant (*red asterisks* represent statistical analyses of neurons on laminin, and *blue* n.s. represents those on PDL). Axon lengths among laminin-coated substrates or PDL-coated substrates were analyzed by ANOVA with Tukey's post hoc test. Axon lengths between laminin-coated and PDL-coated substrates were examined by Student's *t*-test. To see this figure in color, go online.

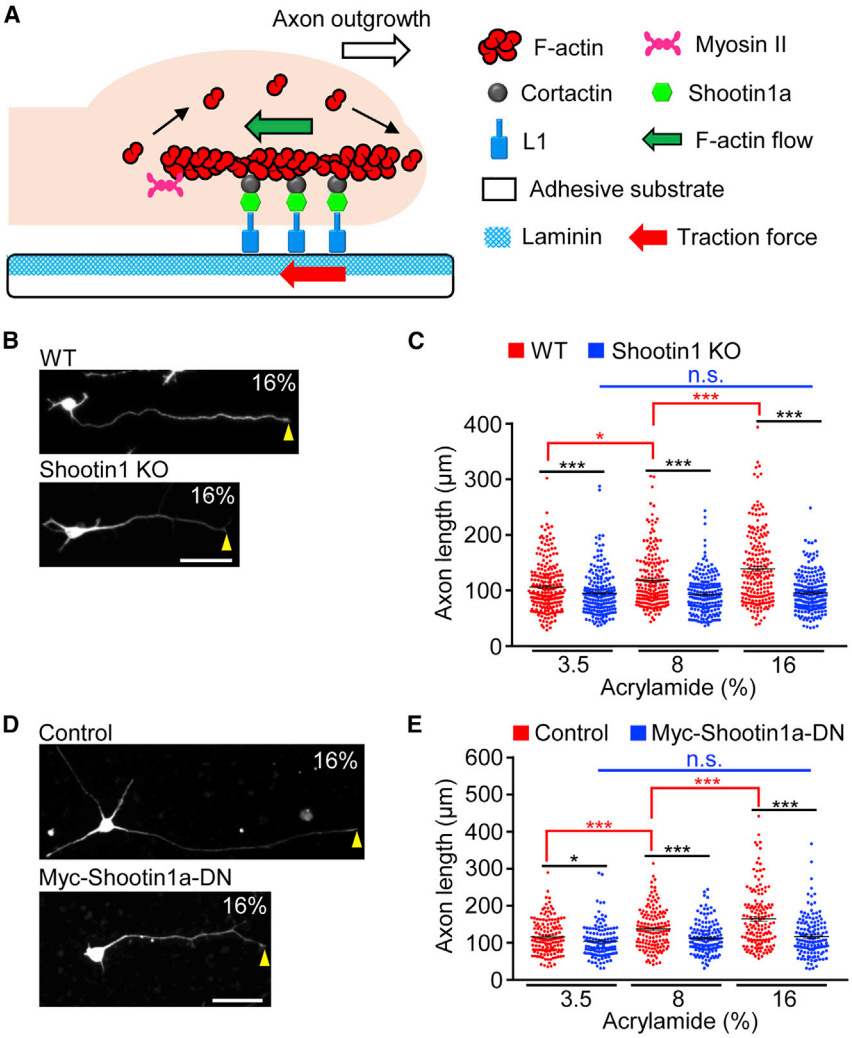

FIGURE 2 Mechanosensitive axon outgrowth requires shootin1a-mediated actin-adhesion coupling. (*A*) Diagram showing the growth cone clutch machinery for axon outgrowth, involving F-actin, myosin II, cortactin, shootin1a, L1, and laminin (31). (*B*) Images of WT and shootin1 KO hippocampal neurons cultured on 16% polyacrylamide gels for 48 h and stained with anti-βIII-tubulin antibody. Arrowheads indicate axonal tips. (*C*) Statistical analysis of axon length of WT and shootin1 KO hippocampal neurons cultured on laminin-coated 3.5, 8, and 16% polyacrylamide gels for 48 h. (WT 3.5%, n = 238 neurons; 8%, n = 205 neurons; 16%, n = 208 neurons; KO 3.5%, n = 206 neurons; 8%, n = 203 neurons; 16%, n = 208 neurons.) (*D*) Hippocampal neurons overexpressing myc-GST (control) or myc-shootin1a-DN were cultured on 16% polyacrylamide gels for 48 h and stained with anti-myc antibody. Arrowheads indicate axonal tips. (*E*) Statistical analysis of axon length of neurons overexpressing myc-GST (control) and neurons overexpressing myc-shootin1a-DN cultured on laminin-coated 3.5, 8, and 16% polyacrylamide gels. (myc-GST 3.5%, n = 153 neurons; 8%, n = 147 neurons; 16%, n = 149 neurons; myc-shootin1a-DN 3.5%, n = 132 neurons; 8%, n = 150 neurons; 16%, n = 149 neurons.) Scale bars, 50 μm. Data in (*C*) and (*E*) represent means ± SE; $*p < 0.05$; $***p < 0.01$; n.s., nonsignificant (*blue* n.s. in *C* represents statistical analyses of shootin1 KO neurons, whereas that in *E* represents statistical analyses of neurons overexpressing myc-shootin1a-DN). Axon lengths between WT and KO neurons or between neurons overexpressing myc-GST and myc-shootin1a-DN were examined by Student's *t*-test. Axon lengths among different substrates were analyzed by ANOVA with Tukey's post hoc test. To see this figure in color, go online.

monitored as a decrease in F-actin retrograde flow speed (12,46,47). As shown in Fig. 3, *A* and *B*, the speed of F-actin retrograde flow decreased significantly with increasing substrate stiffness; the flow speed was 3.6 ± 0.1, 2.9 ± 0.1, and 1.9 ± 0.1 μm/min on laminin-coated 3.5, 8, and 16% gels, respectively. These data indicate that an increase in substrate stiffness promotes actin-adhesion coupling.

We also analyzed the traction force generated by axonal growth cones using traction force microscopy. Neurons were cultured on laminin-coated polyacrylamide gels with embedded 200-nm fluorescent beads. The traction force was monitored by visualizing the deformation of the gel, which is reflected by the displacement of the beads from their original positions. The reporter beads in 3.5 and 8% gels moved dynamically under axonal growth cones (Fig. 3, *C* and *D*; Video S2). Fig. S2 *A* shows a typical movement of the reporter bead in a 3.5% gel. As reported (14), the beads moved in a load (*dashed line*) and fail (*arrowheads*) manner; the mean speed of the bead movement during the load phase on 3.5% gels was 0.58 ± 0.04 μm/min (Fig. S2 *B*).

The magnitude of the traction force calculated by bead displacement was 4.4 ± 0.6 pN/μm^2 on 3.5% gel and 18.5 ± 2.7 pN/μm^2 on 8% gel, and significantly higher on 8% gel than on 3.5% gel (Fig. 3 *E*). On the other hand, we could not detect distinct bead movements on 16% gel (data not shown). The traction forces produced by growth cones (1–40 pN/μm^2) (Fig. 3 *E*) are consistent with previous data (16,24,35) and more than 10 times smaller than those produced by non-neuronal cells, including epithelial cells, smooth muscle cells, fibroblasts, and keratocytes (16). Thus, growth cones are thought of as weak force generators (48). We expect that growth cones produce larger forces on 16% gels, as actin-adhesion is increased on 16% gels (Fig. 3 *B*). However, we consider that the weak traction forces produced by growth cones were not sufficient to distinctly deform 16% gels, which are ~2.7 times stiffer than 8% gels (Fig. S1 *A*). Together, these data suggest that axonal

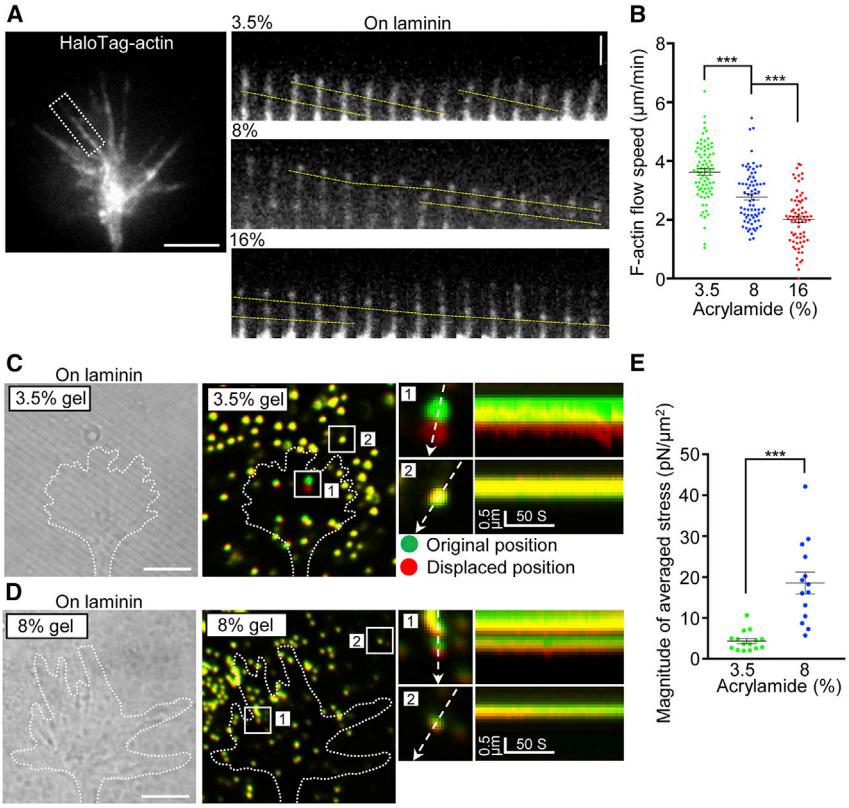

FIGURE 3 Increase in substrate stiffness promotes actin-adhesion coupling and traction force on the substrate. (*A*) A fluorescent feature image (*left*) of HaloTag-actin in axonal growth cones of neurons cultured on laminin-coated 8% polyacrylamide gel (*left*) (see Video S1) and time-lapse montages (*right*) of fluorescent features of HaloTag-actin in filopodia of axonal growth cones on laminin-coated 3.5, 8, and 16% gels at 5-s intervals (*right*, F-actin flows are indicated by *dashed yellow lines*). (*B*) F-actin retrograde flow speeds obtained from the time-lapse montage analyses in (*A*) (3.5%, n = 86 signals; 8%, n = 78 signals; 16%, n = 80 signals). (*C* and *D*) Brightfield (*left panels*) and fluorescence (*middle panels*) images showing axonal growth cones of hippocampal neurons cultured for 1 day on laminin-coated 3.5% (*C*) or 8% (*D*) polyacrylamide gel with embedded 200-nm fluorescent beads (see Video S2). The pictures show representative images from time-lapse series taken every 3 s for 147 s. The original and displaced positions of the beads in the gel are indicated by green and red colors, respectively. Dashed lines indicate the boundary of the growth cones. The time-lapse montages (*right panels*) along the axis of bead displacement (*dashed arrows*) in the indicated areas 1 and 2 of the growth cone show movement of beads recorded every 3 s. The beads in area 2 are reference beads. (*E*) Magnitude of averaged stress of axonal growth cones on laminin-coated 3.5 and 8% polyacrylamide gels (3.5%, n = 15 growth cones; 8%, n = 14 growth cones). Scale bars, 5 μm (in the time-lapse montage of *A*, 2 μm). Data in (*B*) and (*E*) represent means ± SE; ***$p < 0.01$. F-actin retrograde flow speeds were analyzed by ANOVA with Tukey's post hoc test. Magnitudes of averaged stress were examined by Student's *t*-test. To see this figure in color, go online.

growth cones generate larger traction force for axon outgrowth on stiffer substrates by promoting the efficiency of actin-adhesion coupling.

Increase in substrate stiffness promotes L1-laminin interaction

To more precisely identify the clutch interface responsible for the mechanosensitive actin-adhesion coupling, we monitored the movement of L1, which links shootin1a and laminin as a cell adhesion molecule (Fig. 2 *A*). L1-HaloTag expressed in hippocampal neurons was labeled by tetramethylrhodamine ligand and observed with a fluorescence microscope (Fig. 4 *A*; Video S3). As reported previously (31), two phases of L1 signals were observed: immobile L1 puncta (grip phase) (*pink dashed lines*, Fig. 4 *A*) and retrogradely flowing L1 puncta (slip phase) (*blue dashed lines*). The mean speed of L1 slip on 3.5% gels was 3.74 ± 0.06 μm/min and substantially faster than that of the bead movement, which represents the deformation of polyacrylamide gels (Fig. S2 *B*). Therefore, it is unlikely that the L1 slip phase was caused by local gel deformation.

Strikingly, the grip phase of L1 was increased on laminin-coated stiffer substrates (Fig. 4, *A* and *B*); the ratio of the grip phase on laminin-coated 3.5, 8, and 16% gels was 18.8, 30.7, and 46.4%, respectively. Accordingly, the ratio of the slip phase and mean L1 retrograde flow speed decreased on the stiffer substrates (Fig. 4, *B* and *C*). Fig. 4, *D* and *E* show a histogram and the means of the duration time of individual L1 grip phases on the substrates; the duration time of grip phases increased significantly on stiffer substrates. On the other hand, the ratio of the L1 grip phase and duration time of individual L1 grip phases did not show stiffness dependency when neurons were cultured on gels without laminin (Fig. 5), whereas mean L1 retrograde flow speed increased slightly on 8% gels. Together, these data indicate that an increase in substrate stiffness promotes the interaction between L1 and laminin on the substrate.

DISCUSSION

We have shown that cultured hippocampal neurons extend longer axons on stiffer adhesive substrates coated with laminin. We demonstrate that the stiffness-dependent axon

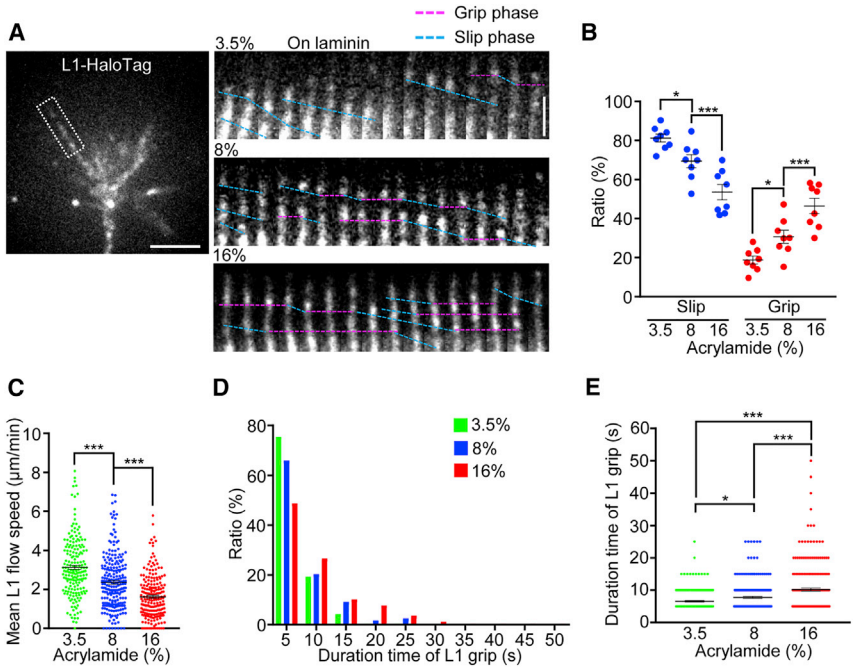

FIGURE 4 Increase in substrate stiffness prolongs the duration of the L1 grip phase. (*A*) A fluorescent feature image (*left*) of L1-HaloTag in axonal growth cone cultured on laminin-coated 8% polyacrylamide gel (see Video S3). Time-lapse montages (*right*) of retrograde flow of L1-HaloTag fluorescent features on laminin-coated 3.5, 8, and 16% gels at 5-s intervals (grip and slip phases are shown by *dashed pink* and *blue lines*, respectively), are given. (*B*) Ratio of grip/slip phases of L1 in growth cones on laminin-coated polyacrylamide gels (3.5%, n = 8 growth cones; 8%, n = 8 growth cones; 16%, n = 8 growth cones). (*C*) Mean retrograde flow speed of L1-HaloTag in axonal growth cones on laminin-coated polyacrylamide gels (3.5%, n = 188 signals; 8%, n = 232 signals; 16%, n = 205 signals). (*D*) Histogram showing the distribution of duration time of L1-HaloTag grip phase. (*E*) Duration time of L1-HaloTag grip phase on laminin-coated polyacrylamide gels (3.5%, n = 232 grip phases; 8%, n = 226 grip phases; 16%, n = 244 grip phases). Scale bars, 5 μm (in the time-lapse montage of *A*, 2 μm). Data in (*B*), (*C*), and (*E*) represent means ± SE; $*p < 0.05$; $***p < 0.01$; n.s., nonsignificant. Data were analyzed by ANOVA with Tukey's post hoc test. To see this figure in color, go online.

outgrowth requires actin-adhesion coupling mediated by the clutch molecule shootin1a, the cell adhesion molecule L1, and the adhesive ligand laminin. L1 at the growth cone membrane underwent grip and slip on the laminin-coated substrate. The duration of the grip phase was extended on stiffer substrates in a laminin-dependent manner, indicating that stiffer substrates promote the interaction between L1 and laminin. Consistent with this, both the actin-adhesion coupling and the traction force exerted on the substrate were increased on stiffer substrates. These data indicate that the stiffness-dependent L1-laminin interaction mediates this mechanosensitivity of the growth cone machinery for axon outgrowth of hippocampal neurons.

Shootin1a-dependent mechanosensitive axon outgrowth of hippocampal neurons

Previous studies have analyzed axon outgrowth of hippocampal neurons cultured on laminin-coated substrates of different stiffnesses, with variable results. Kostic et al. reported that softer gels promoted axon outgrowth (23). On the other hand, Koch et al. reported that stiffer gels increased the traction force produced by growth cones and that the substrate stiffness had no marked influence on total neurite length (24). Our data appear consistent with the latter in this range of stiffness values. Namely, shootin1a is preferentially accumulated in the axonal growth cone of hippocampal neurons cultured for 2 days, but not in the growth cones of other neurites (37). Therefore, shootin1a preferentially promotes traction force at the axonal growth cone. However, as the materials constituting neurite shafts, such as tubulin and plasma membrane, are limited in neurons with rapidly extending axons (37,49,50), an increase in traction force at the axonal growth cone would not necessarily increase substantially the total neurite length. Indeed, the promotion of shootin1a activity by its overexpression does not lead to a substantial increase in the total neurite length of hippocampal neurons (37). Thus, the data indicating that an increase in the substrate stiffness promotes axon outgrowth (Fig. 1, *A* and *B*), but not substantially total neurite length (Fig. S1 *C*) (24), are consistent with the shootin1a-dependent mechanosensitive axon outgrowth (Fig. 2, *B–D*).

Soft molecular clutch for mechanosensitive axon outgrowth

The molecular clutch between F-actin retrograde flow and adhesive substrates has been proposed to contribute to cellular mechanosensing (14,27,28). For example, at focal adhesions of non-neuronal cells, talin and vinculin mediate mechanical coupling between F-actin retrograde flow and integrins as clutch molecules (46,47,51). Talin is thought to be stretched under mechanical tension and on stiffer substrates, thereby recruiting vinculin (52–55). A clutch model originally developed by Chan and Odde (14) and advanced by Roca-Cusachs et al. incorporates the talin-unfolding and vinculin-binding processes into "load and fail" and "frictional slippage" regimes of clutch engagement (14,55). This model excellently describes the mechanoresponse mediated by fibroblasts, in which the cells produce talin-dependent strong traction force above ~80 pN/μm^2 (equivalent to Pa), which increases with increasing substrate

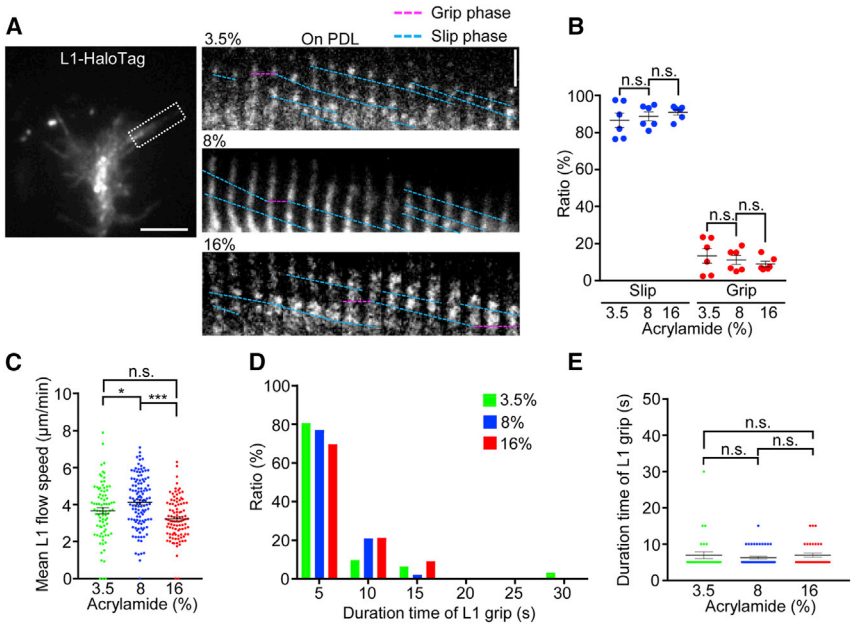

FIGURE 5 Stiffness-dependent increase in the duration of the L1 grip phase requires laminin on the substrate. (*A*) A fluorescent feature image (*left*) of L1-HaloTag in an axonal growth cone cultured on PDL-coated 8% polyacrylamide gel. Time-lapse montages (*right*) of retrograde flow of L1-HaloTag fluorescent features on PDL-coated 3.5, 8, and 16% gels at 5-s intervals (grip and slip phases are shown by *dashed pink* and *blue lines*, respectively) are given. (*B*) Ratio of grip/slip phases of L1 in growth cones on PDL-coated polyacrylamide gels (3.5%, n = 6 growth cones; 8%, n = 6 growth cones; 16%, n = 6 growth cones). (*C*) Mean retrograde flow speed of L1-HaloTag in axonal growth cones on PDL-coated polyacrylamide gels (3.5%, n = 84 signals; 8%, n = 120 signals; 16%, n = 100 signals). (*D*) Histogram showing the distribution of duration time of L1-HaloTag grip phase. (*E*) Duration time of L1-HaloTag grip phase on PDL-coated polyacrylamide gels (3.5%, n = 31 grip phases; 8%, n = 48 grip phases; 16%, n = 33 grip phases). Scale bars, 5 μm (in the time-lapse montage of *A*, 2 μm). Data in (*B*), (*C*), and (*E*) represent means ± SE; $*p < 0.05$; $***p < 0.01$; n.s., nonsignificant. Data were analyzed by ANOVA with Tukey's post hoc test. To see this figure in color, go online.

stiffness (55). This talin-dependent mechanoresponse is further accompanied by the growth of focal adhesions and YAP nuclear translocation (55).

However, it is also reported that the depletion of vinculin paradoxically promotes fibroblast migration in two-dimensional environments (47,56) where vinculin and talin promote clutch coupling and traction force (46,47). In addition, a study with micro-CALI (chromophore-assisted laser inactivation) analyses reported that inactivation of talin or vinculin had no significant effect on neurite outgrowth of chick dorsal root ganglia neurons, although their inactivation affected filopodial motility (57). Therefore, although talin and vinculin provide a key clutch linkage that mediates integrin-based focal adhesion functions, including mechanotransduction (28,53,58,59), it is not precisely understood whether mechanosensitive axon outgrowth requires these molecules. An explanation for the promoted cell migration upon talin depletion might be the strong traction forces produced by the integrin-talin-vinculin clutch system (16,55). Establishment of a strong traction force inevitably requires formation of a strong adhesion that could inhibit cell migration (60,61).

Fibroblasts are also reported to show a talin-independent mechanoresponse in a weak force regime; they produced a weak traction force (below ~80 pN/μm^2), which increased monotonically with increasing substrate stiffness below the threshold of talin unfolding (55). Brain is softer than other tissues such as connective tissues (16–18), and growth cones produce soft and weak traction forces (below ~80 pN/μm^2) (16,35,48). Consistently, our data demonstrate that the mechanosensing mediated by the actin-cortactin-shootin1a-L1-laminin clutch occurs in a weak force regime (Fig. 3 *E*). Thus, we consider that this clutch system mediates a soft mechanosensing for axon outgrowth, which probably occurs below the threshold of talin unfolding.

Catch bond as a possible mechanism to promote the L1-laminin clutch interface

How does the grip phase between L1 and laminin increase on stiffer substrates? At the growth cone membrane, the force generated by actomyosin contraction and F-actin polymerization is transmitted through F-actin retrograde flow (*green arrow*, Fig. 6 *A*), cortactin and shootin1a to L1, thereby pulling the bond between L1 and laminin (*blue arrows*). When this force exceeds a threshold, the bond breaks and L1 slips retrogradely on the substrate (*blue dashed lines*, Fig. 4 *A*) (31). One possible mechanism to explain this mechanosensitivity is the catch bond, in which the average bond lifetime between molecules increases with tensile force (62–65). Studies using single-molecule dynamic force spectroscopy have reported catch bonds between various molecules, such as integrins and their ligand fibronectin (64–66). In addition, it has been proposed that an increase in the rigidity of an adhesive substrate promotes the force-loading rate exerted through a molecular clutch (*blue arrows*, Fig. 6 *B*) (28,55). Hence, we expect that the increase in the L1-laminin grip phase on stiffer substrates reflects catch-bond-like behavior in the L1-laminin interaction on living cells. Although spectroscopy experiments with exogenously applied force demonstrated that different force application histories can elicit distinct dynamic bond types (65,67), endogenous force derived from F-actin retrograde flow is applied to the L1-laminin interaction in this case. Therefore, we consider that a catch-bond-like L1-laminin interaction occurs under physiological conditions (Fig. 6).

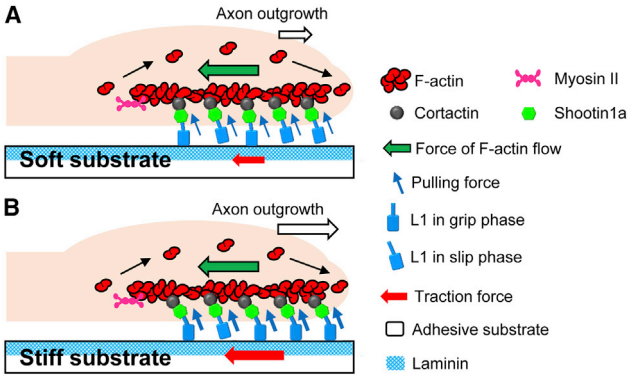

FIGURE 6 A model for mechanosensitive axon outgrowth mediated by catch-bond-like L1-laminin clutch interface. (*A*) The force generated by actomyosin contraction and F-actin polymerization is transmitted through F-actin retrograde flow (*green arrow*), cortactin, and shootin1a to L1, thereby pulling the bond between L1 and laminin (*blue arrows*). When this force exceeds a threshold, the bond breaks and L1 slips retrogradely on the substrate (slip phase). (*B*) An increase in the substrate rigidity promotes the force-loading rate exerted through the molecular clutch (*blue arrows*). This, in turn, induces catch-bond-like behavior of the L1-laminin clutch interface, in which the average bond lifetime between L1 and laminin increases with tensile force, thereby promoting the L1 grip phase, actin-adhesion coupling, traction force (*red arrow*), and axon outgrowth (*white arrow*). To see this figure in color, go online.

Alternatively, we do not rule out the possibility that the L1-laminin interaction is promoted by mechanosensitive cell signaling. Previous studies reported that substrate stiffness modulates the activities of signaling molecules, including focal adhesion kinase (68,69), mechanosensitive ion channels (25,70), calcium (70,71), and RhoA (26,72), in neurons. Signaling downstream of these molecules might promote the L1-laminin interaction by changing the L1 structure. Further mechanistic analyses are required for a precise understanding of how the L1-laminin interaction is regulated.

The molecular clutch as a mechanointegrator for axon guidance

In the brain, axon outgrowth and pathfinding are regulated by diffusible and substrate-bound chemical cues (1,2), in processes called chemotaxis and haptotaxis (73,74). Although the precise role of the mechanosensitive growth cone response remains unclear, environmental mechanical cues are proposed to contribute to axon outgrowth and pathfinding in vivo (25,75); cell movement guided by the stiffness of the substrate is referred to as durotaxis (76).

Recent studies have reported that the molecular clutch system involving shootin1a, cortactin, and L1 mediates axon guidance in response to the diffusible chemotactic ligand netrin-1 (34) and the substrate-bound haptotactic ligand laminin (31). The clutch molecule shootin1 is also involved in the generation of force for neuronal migration (77,78) and required for axon pathfinding and cell migration in vivo in three-dimensional environments (34,77,79). Netrin-1 signals promote Pak1-mediated shootin1a phosphorylation in axonal growth cones under the activation of Cdc42 and Rac1 (12). This, in turn, enhances the clutch linkages between shootin1a and cortactin (35) and shootin1a and L1 (34), thereby promoting traction force for axon outgrowth and chemotaxis (34,35). On the other hand, the regulation of the clutch coupling between L1 and laminin plays a key role in laminin-induced axonal haptotaxis (31). Thus, these findings lead us to propose that the clutch interfaces involving shootin1a, cortactin, L1, and laminin (Fig. 6) respond not only to chemotactic and haptotactic chemical cues but also to durotactic mechanical cues, thereby providing an integrated view of a growth cone machinery for axon outgrowth and pathfinding.

SUPPORTING MATERIAL

Supporting material can be found online at https://doi.org/10.1016/j.bpj.2021.08.009.

AUTHOR CONTRIBUTIONS

K.A., K.B., L.H., K.T.W., and K.O. performed the experiments. K.A., K.B., L.H., and K.T.W. analyzed the data. K.A., L.H., K.B., K.T.W., K.O., Y.H., and N.I. designed the experiments. K.A. and N.I. wrote the manuscript. N.I. supervised all the projects. All authors discussed the results and commented on the manuscript.

ACKNOWLEDGMENTS

We thank Eri Akita for supporting AFM experiments; Dr. Yuichi Sakumura for valuable discussions; Dr. Takunori Minegishi for reading the manuscript; and Qiu Zhen, Singh Saranpal, and Mieko Ueda for supporting data analyses.

This research was supported in part by Japan Agency for Medical Research and Development (AMED) under grant number 21gm0810011h0005 (N.I. and Y.H.), Japan Society for the Promotion of Science (JSPS) KAKENHI (JP19H03223, N.I.), and JSPS Grants-in-Aid for Early-Career Scientists (JP19K16127, K.B.).

REFERENCES

1. Lowery, L. A., and D. Van Vactor. 2009. The trip of the tip: understanding the growth cone machinery. *Nat. Rev. Mol. Cell Biol.* 10:332–343.
2. Kolodkin, A. L., and M. Tessier-Lavigne. 2011. Mechanisms and molecules of neuronal wiring: a primer. *Cold Spring Harb. Perspect. Biol.* 3:a001727.
3. Gomez, T. M., and P. C. Letourneau. 2014. Actin dynamics in growth cone motility and navigation. *J. Neurochem.* 129:221–234.
4. Miller, K. E., and D. M. Suter. 2018. An integrated cytoskeletal model of neurite outgrowth. *Front. Cell. Neurosci.* 12:447.
5. Franze, K. 2020. Integrating chemistry and mechanics: the forces driving axon growth. *Annu. Rev. Cell Dev. Biol.* 36:61–83.
6. Forscher, P., and S. J. Smith. 1988. Actions of cytochalasins on the organization of actin filaments and microtubules in a neuronal growth cone. *J. Cell Biol.* 107:1505–1516.

7. Okabe, S., and N. Hirokawa. 1991. Actin dynamics in growth cones. *J. Neurosci.* 11:1918–1929.
8. Katoh, K., K. Hammar, …, R. Oldenbourg. 1999. Birefringence imaging directly reveals architectural dynamics of filamentous actin in living growth cones. *Mol. Biol. Cell.* 10:197–210.
9. Medeiros, N. A., D. T. Burnette, and P. Forscher. 2006. Myosin II functions in actin-bundle turnover in neuronal growth cones. *Nat. Cell Biol.* 8:215–226.
10. Mitchison, T., and M. Kirschner. 1988. Cytoskeletal dynamics and nerve growth. *Neuron.* 1:761–772.
11. Suter, D. M., and P. Forscher. 2000. Substrate-cytoskeletal coupling as a mechanism for the regulation of growth cone motility and guidance. *J. Neurobiol.* 44:97–113.
12. Toriyama, M., S. Kozawa, …, N. Inagaki. 2013. Conversion of a signal into forces for axon outgrowth through Pak1-mediated shootin1 phosphorylation. *Curr. Biol.* 23:529–534.
13. Mogilner, A., and G. Oster. 1996. Cell motility driven by actin polymerization. *Biophys. J.* 71:3030–3045.
14. Chan, C. E., and D. J. Odde. 2008. Traction dynamics of filopodia on compliant substrates. *Science.* 322:1687–1691.
15. Kerstein, P. C., R. H. Nichol, IV, and T. M. Gomez. 2015. Mechanochemical regulation of growth cone motility. *Front. Cell. Neurosci.* 9:244.
16. Moore, S. W., P. Roca-Cusachs, and M. P. Sheetz. 2010. Stretchy proteins on stretchy substrates: the important elements of integrin-mediated rigidity sensing. *Dev. Cell.* 19:194–206.
17. Tyler, W. J. 2012. The mechanobiology of brain function. *Nat. Rev. Neurosci.* 13:867–878.
18. Barnes, J. M., L. Przybyla, and V. M. Weaver. 2017. Tissue mechanics regulate brain development, homeostasis and disease. *J. Cell Sci.* 130:71–82.
19. Elkin, B. S., E. U. Azeloglu, …, B. Morrison, III. 2007. Mechanical heterogeneity of the rat hippocampus measured by atomic force microscope indentation. *J. Neurotrauma.* 24:812–822.
20. Christ, A. F., K. Franze, …, J. Guck. 2010. Mechanical difference between white and gray matter in the rat cerebellum measured by scanning force microscopy. *J. Biomech.* 43:2986–2992.
21. Koser, D. E., E. Moeendarbary, …, K. Franze. 2015. CNS cell distribution and axon orientation determine local spinal cord mechanical properties. *Biophys. J.* 108:2137–2147.
22. Antonovaite, N., S. V. Beekmans, …, D. Iannuzzi. 2018. Regional variations in stiffness in live mouse brain tissue determined by depth-controlled indentation mapping. *Sci. Rep.* 8:12517.
23. Kostic, A., J. Sap, and M. P. Sheetz. 2007. RPTPalpha is required for rigidity-dependent inhibition of extension and differentiation of hippocampal neurons. *J. Cell Sci.* 120:3895–3904.
24. Koch, D., W. J. Rosoff, …, J. S. Urbach. 2012. Strength in the periphery: growth cone biomechanics and substrate rigidity response in peripheral and central nervous system neurons. *Biophys. J.* 102:452–460.
25. Koser, D. E., A. J. Thompson, …, K. Franze. 2016. Mechanosensing is critical for axon growth in the developing brain. *Nat. Neurosci.* 19:1592–1598.
26. Nichol, R. H., IV, T. S. Catlett, …, T. M. Gómez. 2019. Environmental elasticity regulates cell-type specific RHOA signaling and neuritogenesis of human neurons. *Stem Cell Reports.* 13:1006–1021.
27. Bangasser, B. L., G. A. Shamsan, …, D. J. Odde. 2017. Shifting the optimal stiffness for cell migration. *Nat. Commun.* 8:15313.
28. Elosegui-Artola, A., X. Trepat, and P. Roca-Cusachs. 2018. Control of mechanotransduction by molecular clutch dynamics. *Trends Cell Biol.* 28:356–367.
29. Dahme, M., U. Bartsch, …, N. Mantei. 1997. Disruption of the mouse L1 gene leads to malformations of the nervous system. *Nat. Genet.* 17:346–349.
30. Kamiguchi, H., M. L. Hlavin, …, V. Lemmon. 1998. Adhesion molecules and inherited diseases of the human nervous system. *Annu. Rev. Neurosci.* 21:97–125.
31. Abe, K., H. Katsuno, …, N. Inagaki. 2018. Grip and slip of L1-CAM on adhesive substrates direct growth cone haptotaxis. *Proc. Natl. Acad. Sci. USA.* 115:2764–2769.
32. Hall, H., S. Carbonetto, and M. Schachner. 1997. L1/HNK-1 carbohydrate- and beta 1 integrin-dependent neural cell adhesion to laminin-1. *J. Neurochem.* 68:544–553.
33. Takei, K., T. A. Chan, …, D. G. Jay. 1999. The neural cell adhesion molecules L1 and NCAM-180 act in different steps of neurite outgrowth. *J. Neurosci.* 19:9469–9479.
34. Baba, K., W. Yoshida, …, N. Inagaki. 2018. Gradient-reading and mechano-effector machinery for netrin-1-induced axon guidance. *eLife.* 7:e34593.
35. Kubo, Y., K. Baba, …, N. Inagaki. 2015. Shootin1-cortactin interaction mediates signal-force transduction for axon outgrowth. *J. Cell Biol.* 210:663–676.
36. Shimada, T., M. Toriyama, …, N. Inagaki. 2008. Shootin1 interacts with actin retrograde flow and L1-CAM to promote axon outgrowth. *J. Cell Biol.* 181:817–829.
37. Toriyama, M., T. Shimada, …, N. Inagaki. 2006. Shootin1: a protein involved in the organization of an asymmetric signal for neuronal polarization. *J. Cell Biol.* 175:147–157.
38. Moshayedi, P., L. d. F. Costa, …, K. Franze. 2010. Mechanosensitivity of astrocytes on optimized polyacrylamide gels analyzed by quantitative morphometry. *J. Phys. Condens. Matter.* 22:194114.
39. Elosegui-Artola, A., E. Bazellières, …, P. Roca-Cusachs. 2014. Rigidity sensing and adaptation through regulation of integrin types. *Nat. Mater.* 13:631–637.
40. Zemła, J., J. Bobrowska, …, M. Lekka. 2020. Indenting soft samples (hydrogels and cells) with cantilevers possessing various shapes of probing tip. *Eur. Biophys. J.* 49:485–495.
41. Li, Y., Z. Hu, and C. Li. 1993. New method for measuring Poisson's ratio in polymer gels. *J. Appl. Polym. Sci.* 50:1107–1111.
42. Jurado, C., J. R. Haserick, and J. Lee. 2005. Slipping or gripping? Fluorescent speckle microscopy in fish keratocytes reveals two different mechanisms for generating a retrograde flow of actin. *Mol. Biol. Cell.* 16:507–518.
43. Aratyn-Schaus, Y., and M. L. Gardel. 2010. Transient frictional slip between integrin and the ECM in focal adhesions under myosin II tension. *Curr. Biol.* 20:1145–1153.
44. Sabass, B., M. L. Gardel, …, U. S. Schwarz. 2008. High resolution traction force microscopy based on experimental and computational advances. *Biophys. J.* 94:207–220.
45. Okano, K., A. Matsui, …, H. Masuhara. 2013. In situ laser micropatterning of proteins for dynamically arranging living cells. *Lab Chip.* 13:4078–4086.
46. Zhang, X., G. Jiang, …, M. P. Sheetz. 2008. Talin depletion reveals independence of initial cell spreading from integrin activation and traction. *Nat. Cell Biol.* 10:1062–1068.
47. Thievessen, I., P. M. Thompson, …, C. M. Waterman. 2013. Vinculin-actin interaction couples actin retrograde flow to focal adhesions, but is dispensable for focal adhesion growth. *J. Cell Biol.* 202:163–177.
48. Betz, T., D. Koch, …, J. A. Käs. 2011. Growth cones as soft and weak force generators. *Proc. Natl. Acad. Sci. USA.* 108:13420–13425.
49. Toriyama, M., Y. Sakumura, …, N. Inagaki. 2010. A diffusion-based neurite length-sensing mechanism involved in neuronal symmetry breaking. *Mol. Syst. Biol.* 6:394.
50. Nakazawa, H., T. Sada, …, N. Inagaki. 2012. Rab33a mediates anterograde vesicular transport for membrane exocytosis and axon outgrowth. *J. Neurosci.* 32:12712–12725.
51. Hu, K., L. Ji, …, C. M. Waterman-Storer. 2007. Differential transmission of actin motion within focal adhesions. *Science.* 315:111–115.

52. Riveline, D., E. Zamir, …, A. D. Bershadsky. 2001. Focal contacts as mechanosensors: externally applied local mechanical force induces growth of focal contacts by an mDia1-dependent and ROCK-independent mechanism. *J. Cell Biol.* 153:1175–1186.

53. del Rio, A., R. Perez-Jimenez, …, M. P. Sheetz. 2009. Stretching single talin rod molecules activates vinculin binding. *Science.* 323:638–641.

54. Hirata, H., H. Tatsumi, …, M. Sokabe. 2014. Force-dependent vinculin binding to talin in live cells: a crucial step in anchoring the actin cytoskeleton to focal adhesions. *Am. J. Physiol. Cell Physiol.* 306:C607–C620.

55. Elosegui-Artola, A., R. Oria, …, P. Roca-Cusachs. 2016. Mechanical regulation of a molecular clutch defines force transmission and transduction in response to matrix rigidity. *Nat. Cell Biol.* 18:540–548.

56. Xu, W., H. Baribault, and E. D. Adamson. 1998. Vinculin knockout results in heart and brain defects during embryonic development. *Development.* 125:327–337.

57. Sydor, A. M., A. L. Su, …, D. G. Jay. 1996. Talin and vinculin play distinct roles in filopodial motility in the neuronal growth cone. *J. Cell Biol.* 134:1197–1207.

58. Changede, R., X. Xu, …, M. P. Sheetz. 2015. Nascent integrin adhesions form on all matrix rigidities after integrin activation. *Dev. Cell.* 35:614–621.

59. Sun, Z., S. S. Guo, and R. Fässler. 2016. Integrin-mediated mechanotransduction. *J. Cell Biol.* 215:445–456.

60. Palecek, S. P., J. C. Loftus, …, A. F. Horwitz. 1997. Integrin-ligand binding properties govern cell migration speed through cell-substratum adhesiveness. *Nature.* 385:537–540.

61. Liu, Y. J., M. Le Berre, …, M. Piel. 2015. Confinement and low adhesion induce fast amoeboid migration of slow mesenchymal cells. *Cell.* 160:659–672.

62. Guo, B., and W. H. Guilford. 2006. Mechanics of actomyosin bonds in different nucleotide states are tuned to muscle contraction. *Proc. Natl. Acad. Sci. USA.* 103:9844–9849.

63. Thomas, W. 2008. Catch bonds in adhesion. *Annu. Rev. Biomed. Eng.* 10:39–57.

64. Kong, F., A. J. García, …, C. Zhu. 2009. Demonstration of catch bonds between an integrin and its ligand. *J. Cell Biol.* 185:1275–1284.

65. Zhu, C., Y. Chen, and L. A. Ju. 2019. Dynamic bonds and their roles in mechanosensing. *Curr. Opin. Chem. Biol.* 53:88–97.

66. Chen, Y., H. Lee, …, C. Zhu. 2017. Force regulated conformational change of integrin $\alpha_V\beta_3$. *Matrix Biol.* 60–61:70–85.

67. Sarangapani, K. K., J. Qian, …, C. Zhu. 2011. Regulation of catch bonds by rate of force application. *J. Biol. Chem.* 286:32749–32761.

68. Jiang, F. X., B. Yurke, …, N. A. Langrana. 2008. Neurite outgrowth on a DNA crosslinked hydrogel with tunable stiffnesses. *Ann. Biomed. Eng.* 36:1565–1579.

69. Moore, S. W., X. Zhang, …, M. P. Sheetz. 2012. Netrin-1 attracts axons through FAK-dependent mechanotransduction. *J. Neurosci.* 32:11574–11585.

70. Kerstein, P. C., B. T. Jacques-Fricke, …, T. M. Gomez. 2013. Mechanosensitive TRPC1 channels promote calpain proteolysis of talin to regulate spinal axon outgrowth. *J. Neurosci.* 33:273–285.

71. Franze, K., J. Gerdelmann, …, J. Käs. 2009. Neurite branch retraction is caused by a threshold-dependent mechanical impact. *Biophys. J.* 97:1883–1890.

72. Chang, T. Y., C. Chen, …, P. L. Cheng. 2017. Paxillin facilitates timely neurite initiation on soft-substrate environments by interacting with the endocytic machinery. *eLife.* 6:e31101.

73. Mortimer, D., T. Fothergill, …, G. J. Goodhill. 2008. Growth cone chemotaxis. *Trends Neurosci.* 31:90–98.

74. Carter, S. B. 1967. Haptotaxis and the mechanism of cell motility. *Nature.* 213:256–260.

75. Thompson, A. J., E. K. Pillai, …, K. Franze. 2019. Rapid changes in tissue mechanics regulate cell behaviour in the developing embryonic brain. *eLife.* 8:e39356.

76. Lo, C. M., H. B. Wang, …, Y. L. Wang. 2000. Cell movement is guided by the rigidity of the substrate. *Biophys. J.* 79:144–152.

77. Minegishi, T., Y. Uesugi, …, N. Inagaki. 2018. Shootin1b mediates a mechanical clutch to produce force for neuronal migration. *Cell Rep.* 25:624–639.e6.

78. Minegishi, T., and N. Inagaki. 2020. Forces to drive neuronal migration steps. *Front. Cell Dev. Biol.* 8:863.

79. Urasaki, A., S. Morishita, …, N. Inagaki. 2019. Shootins mediate collective cell migration and organogenesis of the zebrafish posterior lateral line system. *Sci. Rep.* 9:12156.